Computer Physics Communications 62 (1991) 249–266
North-Holland

Simulation and symmetry of shear and elongational flow

M.W. Evans [1] and D.M. Heyes [2]

Department of Chemistry, Royal Holloway and Bedford New College, University of London, Egham, Surrey TW20 OEX, UK

Received 4 September 1989; in revised form 16 January 1990

In this summary of our current research we describe in detail the application of group theory statistical mechanics applied to non-Newtonian shear and elongational flow. We go in some detail into the methodology, with many illustrative examples. We look at shear flow, elongational flow, and then at both simultaneously applied to a model monatomic liquid. We consider both steady state and transient flows and the consequences of the *new* time cross-correlation functions for spectroscopy. We note that a combination of shear and elongational flow can produce a heat flux, the thermal equivalent of the Weissenberg effect.

1. Introduction

This article describes the recent impact of computer simulation and group theoretical statistical mechanics, GTSM, on the study of elongational and shear flow. This is a very rapidly developing area which is expanding our understanding of rheology at the fundamental level, where the dynamics of atoms and molecules are studied directly through the classical (Newtonian and Eulerian) equations of motion. This disposes of the need for semi-empirical constitutive equations [1–5], which do not adequately address the atomic or molecular structure and dynamics of an ensemble under imposed flow. The constitutive equations of traditional rheology bring with them the frame indifference controversy [2], confusing the issues and providing few new insights. The main problem with traditional methods is that they are descriptive rather than prescriptive.

In contrast, recent years have seen the emergence of new simulation algorithms based on novel ways of treating numerically the fundamental equations of motion of flow. Examples are the SLLOD equations developed by D.J. Evans and co-workers [6–10] and also applied by Heyes and co-workers [11–16]; the profile unbiased thermostatting (PUT) methods, outlined later in this article based on the recent work of Heyes, and Brownian dynamics [17,18] (BD) in the study of shear flow. An especially important development in this latter context is the evolution [19] of "second generation" homogeneous deformation programs which can handle complicated combinations of both types of flow. Applications of this approach will be described here.

Using these methods, rheology has finally come to terms with the existence of atoms and molecules. An imposed elongational or laminar stress or an imposed shear stress can be investigated through its effect on individual atomic and molecular dynamical trajectories, worked out on a picosecond time scale and governed by the fundamental equations of motion is the classical approximation. All this is made possible by computers such as the Cray-XMP whose speed and memory capacities are expected to increase considerably. It seems clear therefore that these new simulation methods are destined to complement and replace methods based on constitutive equations, or which

[1] Visiting Academic at IBM, Data Systems Division, Neighborhood Road, Kingston, New York 12401, USA. Also Honorary Research Fellow, Dept. of Physics, Univ. of Lancaster, Lancaster LA1 4YB, UK.

[2] Present address: Department of Chemistry, University of Surrey, Guildford, Surrey GU2 5XH, UK.

otherwise do not use directly the fundamental equations of motion.

With the availability of individual trajectories of atomic or molecular ensembles over typically about half a million time steps, the data reduction process becomes of central importance. Structural changes during elongation or shear flow, or a combination of both, can be displayed visually as in the projections of the instantaneous molecular configurations shown in fig. (1), and an appreciation can be built up in terms of pair radial distribution functions (p.r.d.f.'s), and their angular resolution (see e.g., Heyes and Szczepanski [20]). Angular resolved Cartesian components of the p.r.d.f.'s appear in the laboratory frame (X, Y, Z) when an atomic ensemble is subjected to shear stress, for example. These components are specific indicators of the rheology of the ensemble at the atomic level, and disappear at shear-free equilibrium. There are no direct counterparts from the customary constitutive equations, which therefore lack information on structural changes within the fluid. The traditional language of rheology is "Newtonian" or "non-Newtonian". The fluid is Newtonian if it appears to satisfy Newton's linear relation between stress and strain,

$$\sigma_{XY} = \eta \dot{\gamma}_{XY}, \tag{1}$$

where, σ_{XY} is the XY component of the stress tensor, η is the scalar viscosity and $\dot{\gamma}_{XY} = \partial v_x / \partial Y$, the shear velocity profile. When this is not the case, essentially empirical methods are employed to describe the way in which strain responds to stress. One of the clearest classification schemes

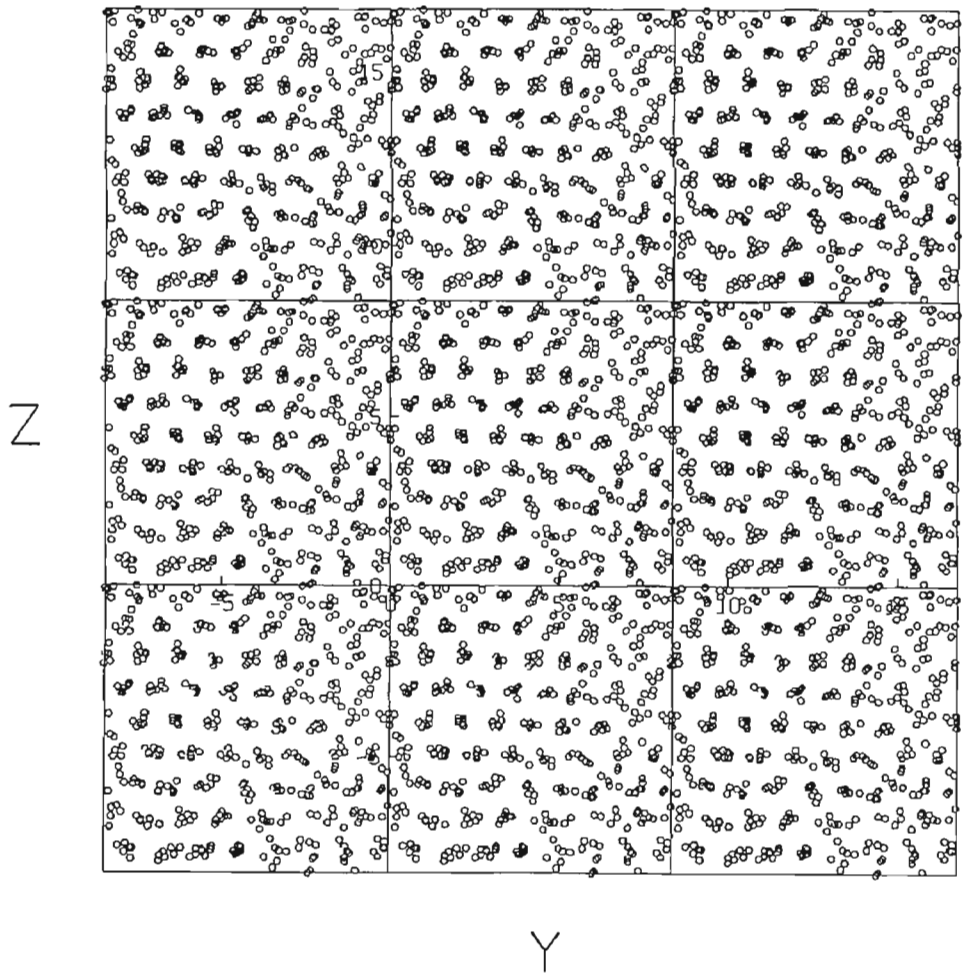

Fig. 1. Scattergrams for 3D sheared LJ fluids at the 3D LJ state $\rho = 0.8442$, $T = 0.722$ with $N = 500$ using the PUT algorithm. The projections of the *centres* of the LJ particles onto the YZ plane are shown. To facilitate the observation of any long-range structure, the real MD cell and surrounding 8 images are given. $\dot{\gamma} = 3.0$.

for non-Newtonian fluids is in terms of the Deborah number, employed by Heyes [18]. Using computer simulation of atomic ensembles, representing "simple" liquids, the non-Newtonian features can be classified in terms of specific and fundamental indicators which are not empirical. The angularly resolved p.r.d.f.'s represent one such set, being thermodynamic ensemble averages built up during the course of the simulation.

The effect of elongation and shear on the dynamics of individual atoms and molecules can be described in terms of time correlation functions, which are Fourier transforms of spectral (frequency) functions through Fourier's integral theorem [21–24]. Correlation functions can be computed at equilibrium, through the equivalence of the ensemble and running time averages of statistical mechanics. Recently, Morriss and Evans [25] have generalised non-linear response and fluctuation dissipation theory with the use of non-equilibrium time correlation functions, which correlate two variables, as usual, but with one at equilibrium and the other in the transient condition after application (or removal) of an external force field. Both equilibrium and non-equilibrium types of time correlation function can be used to reduce the individual trajectories of atoms or molecules to a form where they are in principle observable by spectral methods. Auto correlation functions (a.c.f.'s) are usually identified as involving the product of an atomic or molecular dynamical variable $A(0)$ with $A(t)$, where t is the time. The a.c.f. is

$$C_1(t) = \langle A(0)A(t)\rangle, \tag{2}$$

where $\langle \ldots \rangle$ means "running time average", equivalent to "ensemble average". The quantity A can be a scalar, vector or tensor, and in consequence $A(0)A(t)$ can be a scalar, vector or tensor product. The term "a.c.f." is usually confined to the diagonal elements of such products, for example $\langle A_X(t)A_X(0)\rangle$ and so on. The off = diagonal elements, such as $\langle A_X(t)A_Y(0)\rangle$ are denoted "cross correlation functions" (c.c.f.'s). More generally, a c.c.f. correlates $A(0)$ with another variable $B(t)$ which may refer to the same atom a time t later or a different atom of the ensemble. In this article we deal almost exclusively with c.c.f.'s of this type between two different variables A and B of the same atom. The c.c.f. is, therefore,

$$C_2(t) = \langle A(0)B(t)\rangle \tag{3}$$

(both diagonal and off-diagonal elements). Note that the Fourier transforms of correlation functions (a.c.f's and c.c.f.'s, equilibrium and non-equilibrium) are always spectral functions through Fourier's integral theorem. Some of these spectra are observable experimentally so that time correlation functions indicate directly to what extent a fluid is non-Newtonian. They provide the essential link between observation and computer simulation.

The next section deals with the principles underpinning the *new* simulation advances in non-equilibrium molecular dynamics (NEMD).

2. Group theory statistical mechanics

This branch of statistical mechanics rests on three principles [26–31] with which the well-developed methods of point group theory [32–35] are applied to the ensemble averages exemplified in the introduction. These principles allow conclusions to be drawn on the basis of symmetry alone, without going into further detail, thus providing a powerful and valuable guide to computer simulation, equilibrium and non-equilibrium alike, saving a vast amount of unnecessary computation, and providing valuable new insights in the context of elongational and shear flow at the necessary atomic or molecular level.

Principle (1) is the Neumann or Curie principle [36,37] expressed in the language of contemporary group theory and statistical mechanics. It operates in the laboratory frame, (X, Y, Z). Principle (2) is the equivalent in a frame of reference (x, y, z) defined with respect to the individual molecule of an ensemble, and has been developed from recent work by Whiffen [38]. Principle (3) is concerned with the effect on the symmetry of ensemble averages of applied external force fields of all kinds, and is a powerful, generally applicable and simple statement. Principle (1) states that the thermodynamic ensemble average $\langle ABC\ldots\rangle$ of the atomic or molecular variables $A, B, C, \ldots$ exists in frame

(X, Y, Z) if the product of their individual symmetry representations contains at least once the totally symmetric representation of the point group of the ensemble at field-free thermodynamic equilibrium. Principle (2) states that this average exists in the molecule fixed frame (x, y, z) if the product of representations in the point group of the molecule contains the totally symmetric representation of that point group at least once. Principle (3) states that in the steady state in the presence of an applied field of force, or in the transient condition immediately following the imposition or removal of such a force field, new ensemble averages may appear whose symmetry is that of the applied field.

The application of these principles requires definitions of the appropriate point groups and their irreducible representations from point group theory. The point group of an isotropic ensemble of achiral molecules, or of atoms, at field-free thermodynamic equilibrium is the group of all rotations and reflections, denoted $R_h(3)$. "Reflection" in this context is more accurately defined as the parity inversion operation (X, Y, Z) to $(-X, -Y, -Z)$. The irreducible representations of $R_h(3)$ are denoted,

$$D_g^{(0)}, \ldots, D_g^{(n)} \quad \text{or} \quad D_u^{(0)}, \ldots, D_u^{(n)},$$

where the subscript "g" denotes positive to parity inversion and "u" negative. The D representation of the thermodynamic ensemble average $\langle A \rangle$ is identified within the point group with that of A itself, and is denoted $\Gamma(A)$. The D representation of the c.c.f. $\langle A(t)B(0) \rangle$ is the product of representations $\Gamma(A)\Gamma(B)$.

The totally symmetric irreducible representation of $R_h(3)$ is $D_g^{(0)}$, that of a *scalar* quantity such as mass which is invariant to all rotations and reflections about a point in (X, Y, Z). Vector quantities are polar or axial. The former is denoted $D_u^{(1)}$, and is exemplified by linear centre of mass velocity (v), and the latter is $D_g^{(1)}$, exemplified by molecular angular velocity. A polar vector is negative and an axial vector positive to parity inversion. Tensor quantities are rank (2) onwards in D representation, and may be u or g. Finally, pseudoscalars are $D_u^{(0)}$, and are scalar quantities negative to parity inversion.

Principle (1) applied in $R_h(3)$ implies that the ensemble average $\langle A(t) \rangle$ vanishes for all t unless it contains $D_g(0)$ at least once. This implies that the ensemble average over a pseudoscalar or a vector vanishes at field-free equilibrium. The point group of an ensemble of chiral (optically active) molecules in (X, Y, Z) is the group of all possible rotations, R(3). In this case parity inversion takes the ensemble to its opposite enantiomer, a physically different entity, and is not therefore a valid operation of point group theory. The irreducible representations of R(3) are

$$D(0), \ldots, D(n),$$

without the g and u subscripts of parity inversion. In R(3) the D representations of a scalar and pseudoscalar are both $D^{(0)}$, the totally symmetric irreducible representation. Principle (1) implies that ensemble averages over both scalar and pseudoscalar quantities exist in R(3), an example of the latter being the rotation of plane polarised radiation, positive in one enantiomer and negative in the other. Ensemble averages over all quantities that do not contain $D^{(0)}$ vanish in R(3).

In order to find the D representation of a time correlation function, the Clebsch–Gordan theorem is used,

$$D^{(n)}D^{(m)} = D^{(n+m)} + D^{(n+m-1)} + \cdots + D^{(|n-m|)}. \tag{4}$$

This theorem is valid both for g and u subscripts, the rule for subscript multiplication being

$$gg = g, \qquad gu = ug = u, \qquad uu = g. \tag{5}$$

From eqs. (4) and (5) we have, for example,

$$D_g^{(1)}D_g^{(1)} = D_g^{(0)} + D_g^{(1)} + D_g^{(2)}, \tag{6}$$

or

$$D_g^{(1)}D_u^{(1)} = D_u^{(0)} + D_u^{(1)} + D_u^{(2)}. \tag{7}$$

Equations (6) and (7) express the fact that the product of two vector quantities is in general the sum of three irreducible representations of $R_h(3)$ in frame (X, Y, Z), which are also the representations of the equivalent ensemble averages. The D representation of the correlation function $\langle v(t)v(0) \rangle$ is therefore the right hand side of eq.

(6), and that of $\langle v(t)\omega(0)\rangle$ the right hand side of eq. (7). Here v is molecular centre of mass linear velocity and ω the angular velocity of the same molecule.

We shall see that the correlation function $\langle v(t)v(0)\rangle$ is a key indicator of the response of a fluid to elongational or shear stress. Its D representation in $R_h(3)$ is given by eq. (6), which is valid both for the equilibrium and non-equilibrium (transient) condition. Equation (6) shows that in general there are three parts to $\langle v(t)v(0)\rangle$:
(1) the scalar (dot) product $D_g^{(0)}$;
(2) the vector (cross) product $D_g^{(1)}$;
(3) the tensor (dyadic) product $D_g^{(2)}$.
Principle (1) means that only the dot product exists at field-free equilibrium, this being the a.c.f. $\langle v(t)\cdot v(0)\rangle$. Principle (3) implies that an external field of the right symmetry may result in the appearance of the other two parts of $\langle v(t)v(0)\rangle$, both in the transient condition and in the field-on steady state.

The molecule fixed frame (x, y, z)

The relevant point group in this case is that of the molecule itself, as in the standard point group character tables. Symmetry representations of scalar, vector and tensor quantities can be mapped from frame (X, Y, Z) on to frame (x, y, z) using the mapping rules of point group theory. Some of these mappings for thirty six of the molecular point groups are illustrated in table (1). Quantities which are positive or negative to parity inversion in frame (X, Y, Z) map naturally on to different symmetry representations in (x, y, z). One consequence of this is that c.c.f.'s such as $\langle v(t)\omega(0)\rangle$ which vanish by principle (1) in frame (X, Y, Z) exist in principle (2) for some molecular point groups in frame (x, y, z). The number of scalar elements of the correlation function [39–42] in frame (x, y, z) is given by the number of occurrences (table (1)) of the totally symmetric irreducible representation of the molecular point group. Precise agreement has been obtained between recent computer simulations [40–46] of these elements and principle (2). The last column of table (1) refers to the fact that in molecular crystals, the point group equivalent to (x, y, z) in liquids is one of the thirty two crystallographic point groups. This implies that in crystals, and also in liquid crystals *, principle (2) can be applied to frames other than that of the molecule itself such as that of the nematic, cholesteric or smectic director, with several interesting consequencies.

In future studies of the rheology of molecular (structured) fluids and liquid crystals, the combined use of the three principles and computer simulation will produce a wealth of results inaccessible to the traditional approach. The latter results in a morass of insoluble constitutive equations with many empirical parameters.

In the sections that follow, we review the results obtained already for atomic ensembles subjected to elongational and shear stress, bringing in to operation principle (3) both for the field-on steady state and for transient, nonequilibrium processes.

3. Asymmetric correlation functions

Shear stress (and also elongational stress) is equivalent to an applied force field with a particular D symmetry in frame (X, Y, Z). The response of the atomic ensemble is governed by principle (3). Before dealing with the nature of this response we give some simple examples of the use of this principle in atomic and molecular ensembles subjected to representative force field symmetries.

One of the simplest examples of principle (3) is Newton's second law of motion in an inertial frame, where force results in linear acceleration. Thus a simple linear force imparted to the centre of mass of each molecule of an ensemble results in the acceleration of the ensemble, an ensemble average with the same $D_u^{(1)}$ symmetry as the applied field. A static electric field, again with $D_u^{(1)}$ symmetry, results in polarisation of the dielectric expressed as the development of a non-vanishing ensemble average over the molecular permanent dipole moments, with the same $D_u^{(1)}$ symmetry. A magnetic field of $D_g^{(1)}$ symmetry results in magnetisation, a non vanishing ensemble average over the molecular magnetic dipole moments, again

* See for example the review by J.V. Moscicki [47].

Table 1
Mappings from the (X, Y, Z) frame to thirty six point groups

Point group	Scalar ($D_g^{(0)}$)	Pseudo-scalar ($D_u^{(0)}$)	Axial vector ($D_g^{(1)}$)	Polar vector ($D_u^{(1)}$)	$D_g^{(1)}D_g^{(1)} = D_u^{(1)}D_u^{(1)} = D_g^{(0)} + D_g^{(1)} + D_g^{(2)}$ [a]	$D_u^{(1)}D_g^{(1)} = D_u^{(0)} + D_u^{(1)} + D_u^{(2)}$ [b]	No. [c]	No. [d]	Local symmetry
$C_1(1)$	A	A	3A	3A	9A	9A	9	9	triclinic
$C_i(S_2)(\bar{1})$	A_g	A_u	$3A_g$	$3A_u$	$9A_g$	$9A_u$	9	0	triclinic
$C_2(2)$	A	A	A+2B	A+2B	5A+4B	5A+4B	5	5	monoclinic
$C_{1h}(m)$	A^I	A^{II}	A^I+2A^{II}	$2A^I+A^{II}$	$5A^I+4A^{II}$	$4A^I+5A^{II}$	5	4	monoclinic
$C_{2h}(2/m)$	A_g	A_u	A_g+2B_g	A_u+2B_u	$5A_g+4B_g$	$5A_u+4B_u$	5	0	monoclinic
$C_{2v}(2mm)$	A_1	A_2	$A_2+B_1+B_2$	$A_1+B_1+B_2$	$3A_1+2B_1+2B_2+2A_2$	$2A_1+3A_2+2B_1+B_2$	3	2	orthorhombic
$D_2(232)$	A_1	A_1	$B_1+B_2+B_3$	$B_1+B_2+B_3$	$3A_1+2B_1+2B_2+2B_3$	$3A_1+2B_1+2B_2+2B_3$	3	3	orthorhombic
$D_{2h}(mmm)$	A_{1g}	A_{1u}	$B_{1g}+B_{2g}+B_{3g}$	$B_{1u}+B_{2u}+B_{3u}$	$3A_{1g}+2B_{1g}+2B_{2g}+2B_{3g}$	$3A_{1u}+2B_{1u}+2B_{2u}+2B_{3u}$	3	0	orthorhombic
$C_3(3)$	A	A	A+E	A+E	3A+3E	3A+3E	2	2	trigonal
$C_{3v}(2m)$	A_1	A_2	A_2+E	A_1+E	$2A_1+A_2+3E$	A_1+2A_2+3E	2	1	trigonal
$D_3(32)$	A_1	A_1	A_2+E	A_2+E	$2A_1+A_2+3E$	$2A_1+A_2+3E$	2	2	trigonal
$D_{3d}(\bar{3}m)$	A_{1g}	A_{1u}	$A_{2g}+E_g$	$A_{2u}+E_u$	$2A_{1g}+A_{2g}+3E_g$	$2A_{1u}+A_{2u}+3E_u$	2	0	trigonal
$S_6(\bar{3})$	A_g	A_u	A_g+E_g	A_u+E_u	$3A_g+3E_g$	$3A_u+3E_u$	3	0	trigonal
$C_4(4)$	A	A	A+E	A+E	3A+2B+2E	3A+2B+2E	3	3	tetragonal
$C_{4v}(4mm)$	A_1	A_2	A_2+E	A_1+E	$2A_1+A_2+B_1+B_2+2E$	$A_1+2A_2+B_1+B_2+2E$	2	1	tetragonal
$C_{4h}(4/m)$	A_g	A_u	A_g+E_g	A_u+E_u	$3A_g+2B_g+2E_g$	$3A_u+2B_u+2E_u$	2	0	tetragonal
$D_4(422)$	A_1	A_1	A_2+E	A_2+E	$2A_1+A_2+B_1+B_2+2E$	$2A_1+A_2+B_1+B_2+2E$	2	2	tetragonal
$D_{4h}(4/mmm)$	A_{1g}	A_{1u}	$A_{2g}+E_g$	$A_{2u}+E_u$	$2A_{1g}+A_{2g}+B_{1g}+B_{2g}+2E_g$	$2A_{1u}+A_{2u}+B_{1u}+B_{2u}+2E_u$	2	0	tetragonal
$D_{2d}(\bar{4}2m)$	A_1	B_1	A_2+E	B_2+E	$2A_1+A_2+B_1+B_2+2E$	$A_1+A_2+2B_1+B_2+2E$	2	1	tetragonal
$S_4(\bar{4})$	A	B	A+E	B+E	3A+2B+2E	2A+3B+2E	3	2	tetragonal
$C_6(6)$	A	A	$A+E_1$	$A+E_1$	$3A+2E_1+E_2$	$3A+2E_1+E_2$	3	3	hexagonal
$C_{6v}(6mm)$	A_1	A_2	A_2+E_1	A_1+E_1	$2A_1+A_2+2E_1+E_2$	$A_1+A_2+2E_1+E_2$	2	1	hexagonal
$C_{3h}(\bar{6})$	A^I	A^{II}	A^I+E^{II}	$A^{II}+E^I$	$3A^I+2E^{II}+E^I$	$3A^{II}+3E^{II}$	3	0	hexagonal
$C_{6h}(6/m)$	A_g	A_u	A_g+E_{1g}	A_u+E_{1u}	$3A_g+2E_{1g}+E_{2g}$	$3A_u+2E_{1u}+E_{2u}$	3	0	hexagonal
$D_6(622)$	A_1	A_1	A_2+E_1	A_2+E_1	$2A_1+A_2+E_2+2E_1$	$2A_1+A_2+E_2+2E_1$	2	2	hexagonal
$D_{3h}(6m2)$	A_1^I	A_1^{II}	$A_2^I+E^{II}$	$A_2^{II}+E^I$	$2A_1^I+A_2^I+E^I+2E^{II}$	$2A_1^{II}+A_2^{II}+2E^I+E^{II}$	2	0	hexagonal
$D_{6h}(6/mmm)$	A_{1g}	A_{1u}	$A_{2g}+E_{1g}$	$A_{2u}+E_{1u}$	$2A_{1g}+A_{2g}+2E_{1g}+E_{2g}$	$2A_{1u}+A_{2u}+2E_{1u}+E_{2u}$	2	0	hexagonal
$T_d(\bar{4}3m)$	A_1	A_2	T_1	T_2	$A_1+T_1+E+T_2$	$A_2+T_2+E+T_1$	1	0	cubic
$O_h(m3m)$	A_{1g}	A_{1u}	T_{1g}	T_{1u}	$A_{1g}+T_{1g}+E_g+T_{2g}$	$A_{1u}+T_{1u}+E_u+T_{2u}$	1	0	cubic
T(23)	A	A	T	T	A+E+2T	A+E+2T	1	1	cubic
$T_h(m3)$	A_g	A_u	T_g	T_u	$A_g+E_g+2T_g$	$A_u+E_u+2T_u$	1	0	cubic
O(434)	A_1	A_1	T_1	T_1	$A_1+E+T_1+T_2$	$A_1+E+T_1+T_2$	1	1	cubic
$C_{\infty r}$	Σ^+	Σ^-	$\Sigma^-+\Pi$	$\Sigma^++\Pi$	$2\Sigma^++\Sigma^-+2\Pi+\Delta$	$2\Sigma^-+\Sigma^++2\Pi+\Delta$	2	1	linear dipolar
C_∞	Σ	Σ	$\Sigma+\Pi$	$\Sigma+\Pi$	$3\Sigma+2\Pi+\Delta$	$3\Sigma+2\Pi+\Delta$	3	3	linear dipolar chiral
$D_{\infty h}$	Σ_g^+	Σ_u^-	$\Sigma_g^-+\Pi_g$	$\Sigma_u^++\Pi_w$	$2\Sigma_g^++\Sigma_g^-+2\Pi_g+\Delta_g$	$2\Sigma_w^-+\Sigma_u^++2\Pi_u+\Delta_u$	2	0	linear non-dipolar
D_∞	Σ^+	Σ^+	$\Sigma^-+\Pi$	$\Sigma^-+\Pi$	$2\Sigma^++\Sigma^-+2\Pi+\Delta$	$2\Sigma^-+\Sigma^++2\Pi+\Delta$	2	2	linear non-dipolar chiral

[a] Complete product of two axial vectors.
[b] Complete product of polar and axial vectors.
[c] Number of non-vanishing scalar elements of the tensor product of two axial vectors.
[d] Number of non-vanishing scalar elements of the tensor product of polar and axial vectors.

with the same $D_g^{(1)}$ symmetry. Principle (3) becomes increasingly useful when dealing with more complicated ensemble responses to imposed fields of force. For example it was shown by computer simulation some years ago [47–50] that a static electric field in axis Z of frame (X, Y, Z) results in the appearance of

$$\langle v_X(t)\omega_Y(0)\rangle = -\langle v_Y(t)\omega_X(0)\rangle \tag{8}$$

in the same, laboratory, frame. Principle (3) applies here and explains why this particular c.c.f. symmetry is observed. The electric field symmetry is $D_u^{(1)}$, which is imparted to the *vector* part of $\langle v(t)\omega(0)\rangle$, which has the same $D_u^{(1)}$ symmetry and is the cross product $\langle v(t)\times\omega(0)\rangle$, whose component in Z is $(\langle v_X(t)\omega_Y(0)\rangle - \langle v_Y(t)\omega_X(0)\rangle)\boldsymbol{k}$ by definition, where $\boldsymbol{k}$ is a unit vector in the Z axis. In order for this not to vanish identically, result (8) follows, and is confirmed by the numerical simulation [47–50]. The $D_u^{(1)}$ field symmetry has produced by principle (3) the $D_u^{(1)}$ component of the c.c.f. $\langle v(t)\omega(0)\rangle$, and this component only.

3.1. Symmetry of a shear field

Principle (3) has recently been applied to investigate the response of an atomic ensemble to shear stress in terms of the indicator c.c.f. $\langle v(t)v(0)\rangle$. This has resulted in the discovery [51–54] of new types of correlation function which are neither symmetric nor anti-symmetric in time reversal, thus seeming to violate the cornerstone Onsager–Casimir reciprocal principle for systems at equilibrium [55]. These asymmetric c.c.f.'s appear in response to a stress tensor and shear strain rate of the type,

$$\dot{\gamma} = \partial v_X/\partial Y, \tag{9}$$

which is one component of the tensor vr^{-1}, where v is a velocity vector of $D_u^{(1)}$ symmetry and r^{-1} an inverse position vector of the same D symmetry. The D representation of this product is,

$$\Gamma(v)\Gamma(r^{-1}) = D_g^{(0)} + D_g^{(1)} + D_g^{(2)}, \tag{10}$$

where we have used the Clebsch–Gordan theorem. The force field producing this strain rate has the same symmetry, which by principle (3) produces new ensemble averages of this symmetry in the field-on steady state or in the transient condition. This time it is possible in principle to generate simultaneously all three symmetry types on the right hand side of eq. (10). However, vr^{-1} is traceless in shear flow, and the force field does not include $D_g^{(0)}$. New ensemble averages with the other two D symmetries may appear, however, by principle (3). Shear may therefore produce both the $D_g^{(1)}$ and $D_g^{(2)}$ components of a correlation function such as $\langle v(t)v(0)\rangle$ whose complete D representation is the same as that of the external field symmetry (10). If the shear stress is applied in the plane XY these are

$$\langle v_X(t)v_Y(0)\rangle = -\langle v_Y(t)v_X(0)\rangle, \tag{11a}$$

of $D_g^{(1)}$ symmetry and

$$\langle v_X(t)v_Y(0)\rangle = \langle v_Y(t)v_X(0)\rangle, \tag{11b}$$

of $D_g^{(2)}$ symmetry. The observed response of the indicator c.c.f. $\langle v(t)v(0)\rangle$ is therefore in general a *weighted* combination of eqs. (11a) and (11b), giving the result [52–54]

$$\langle v_X(t)v_Y(0)\rangle \neq \langle v_Y(t)v_X(0)\rangle, \tag{12}$$

This is uniquely indicative of the response at the fundamental level of an atomic ensemble to shear, a new and totally unexpected result of the seemingly simple statement that we have called principle (3).

The c.c.f. (12) is "asymmetric" because it is neither antisymmetric (eq. (11a)) nor symmetric (eq. (11b)) in the interchange of subscripts X and Y, equivalent to shifting the time argument. This occurs even though the sample may be statistically stationary in the shear-on steady state, and despite the fact that the Onsager–Casimir reciprocal principle demands for equilibrium systems either symmetry or antisymmetry in X and Y.

3.2. Simulation details

We used the SLLOD equations of motion to incorporate laminar shear flow in most of the

calculations [11]. The peculiar or thermal velocity is denoted by $\tilde{v}$. For molecular position, $\boldsymbol{R}$,

$$\dot{R}_X = v_X = \tilde{v}_X + \dot{\gamma} R_Y, \tag{13}$$

$$\dot{R}_Y = v_Y = \tilde{v}_Y, \tag{14}$$

$$\dot{R}_Z = v_Z = \tilde{v}_Z, \tag{15}$$

$$\frac{\mathrm{d}\tilde{v}_X}{\mathrm{d}t} = \frac{F_X}{m} - \dot{\gamma}\tilde{v}_Y, \tag{16}$$

$$\frac{\mathrm{d}\tilde{v}_Y}{\mathrm{d}t} = \frac{F_Y}{m}, \tag{17}$$

$$\frac{\mathrm{d}\tilde{v}_Z}{\mathrm{d}t} = \frac{F_Z}{m}, \tag{18}$$

where the α component of the force on a particle is F_α, the velocity is v_α, the peculiar velocity is $\tilde{v}_\alpha$ (i.e. that component of the velocity in excess of the streaming flow velocity). We maintain constant kinetic energy ("temperature") within the Verlet algorithm using velocity rescaling applied to $\tilde{v}_\alpha$. The transient time correlation functions were determined using the method of Evans and Morris [25] with appropriate symmetry mappings of the equilibrium phase state points to reduce the noise at long time.

The MD simulations followed particles of mass, m, interacting via the Lennard-Jones, LJ, potential,

$$\phi(r) = 4\epsilon\left((\sigma/r)^{12} - (\sigma/r)^{6}\right), \tag{19}$$

The basic technique has been described elsewhere [11]. The MD simulations were performed on a cubic unit cell volume V containing $N = 256$ and $N = 500$ for the transient flows and $N = 500$ for the steady-state shear flows. The interactions were truncated at 2.5 σ. We use LJ reduced units throughout, i.e. $k_B T/\epsilon \to T$, and number density, $\rho = N\sigma^3/V$. Time is in $\sigma(m/\epsilon)^{1/2}$, strain rate is in $(\epsilon/m)^{1/2}/\sigma$, viscosity is in $(m\epsilon)^{1/2}/\sigma^2$ and stress is in $\epsilon\sigma^{-3}$. The temperature was fixed by velocity rescaling of the peculiar velocities [56]. The time step was 0.015. The state point mainly considered was a near triple-point state, at $\rho = 0.8442$ and $T = 0.722$. In the sheared case, $\dot{\gamma} = 1.0$, produces $\eta = 2.1$, about 30% shear thinning [12]. The stress and thermodynamic properties are governed mainly by the configurational ($\phi(r)$) dependent terms. Computations were carried out in single precision on a CRAY-XMP at the University of London Computer Centre.

We calculated the shear viscosity, η, from,

$$\eta = -P_{XY}/\dot{\gamma}, \tag{20}$$

where

$$P_{XY} = \frac{1}{V}\left(\sum_{i=1}^{N} m_i \tilde{v}_{xi}\tilde{v}_{yi} - \sum_{i=1}^{N-1}\sum_{j>i}^{N}\left(\frac{r_{xij}r_{yij}}{r_{ij}}\right)\frac{\mathrm{d}\phi(r_{ij})}{\mathrm{d}r}\right), \tag{21}$$

where r_{xij} is the x component of r_{ij} and $V = (N/\rho)$, the volume of the MD cell.

Some simulations were also carried out at steady state using the PUT algorithm [57]. In SLLOD a linear velocity profile $v_X(Y)$ is assumed in the thermostatting procedure. Any deviations from this will be taken as an extra contribution to the temperature and duly suppressed. In PUT no assumption is made about the instantaneous shear velocity distribution within the MD cell. It is therefore more realistic than SLLOD at high shear rates, because it naturally incorporates the local velocity fluctuations about the mean (from the shear rate). Therefore the onset of turbulence is more realistically modelled. Our implementation of the PUT equations of motion differs from that of Evans and Morriss, in determining a local temperature for each particle from its local drift velocity. The instantaneous average drift velocity around each particle is obtained by summing the velocities within an enclosing sphere. A spherical truncation radius of value $r_p = 1.5\ \sigma$ or $2.0\ \sigma$ was typically used. (Properties were only moderately sensitive to values of r_p in this range.)

If the shear strain rate is $\dot{\gamma} = \partial v_X/\partial Y$, the new cross correlations are of the type $\langle v_X(t)v_Y(0)\rangle$, $\langle P_{\alpha X}(t)P_{\alpha Y}(0)\rangle$ and $\langle P_{\alpha\alpha}(t)P_{XY}(0)\rangle$, where $\boldsymbol{v}$ is the atomic velocity in the XYZ frame and $P_{\alpha\beta}$ is the $\alpha\beta$ component of the pressure tensor [11]. That is, $\langle P_{XZ}(0)P_{YZ}(t)\rangle$, $\langle P_{XY}(0)P_{XX}(t)\rangle$, $\langle P_{XY}(0)P_{YY}(t)\rangle$, $\langle P_{XY}(0)P_{ZZ}(t)\rangle$, $\langle P_{XX}(0)P_{XX}(t)\rangle$, $\langle P_{YY}(0)P_{YY}(t)\rangle$ and $\langle P_{ZZ}(0)P_{ZZ}(t)\rangle$. This includes also these c.c.f.'s with time arguments reversed, which as noted can be different functions

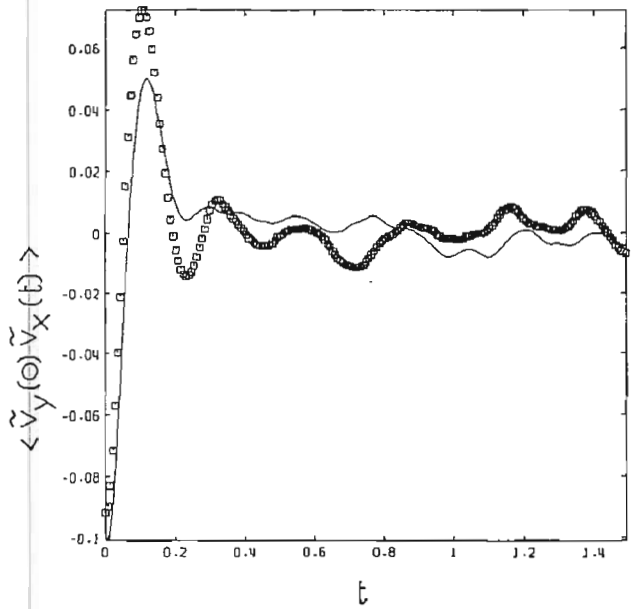

Fig. 2. The peculiar velocity time correlation functions $\langle \tilde{v}_Y(0)\tilde{v}_X(t)\rangle$, solid line, SLLOD, dashed line, PUT, at the 3D LJ $N = 500$ state, $\rho = 0.8442$, $T = 0.722$ and $\dot{\gamma} = 1$. The fluid is subjected to steady-state shear and the correlation functions are steady state.

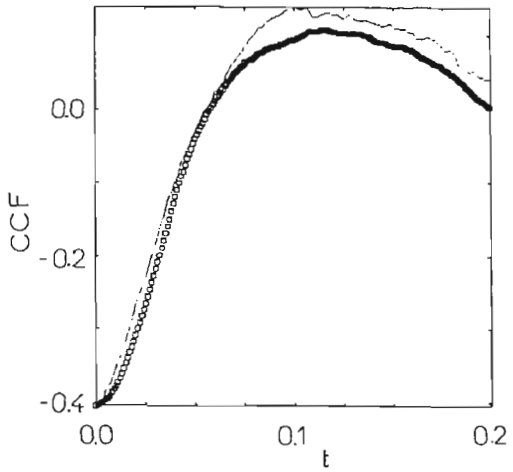

Fig. 3. The peculiar velocity time correlation functions $\langle \tilde{v}_X(0)\tilde{v}_Y(t)\rangle$, solid line, and $\langle \tilde{v}_Y(0)\tilde{v}_X 9t)\rangle$, □, PUT, at the 3D LJ state, $\rho = 0.733$, $T = 1.0$ and $\dot{\gamma} = 5$. The simulations are at steady-state shear. The correlation functions are steady state.

at non-equilibrium. For the purpose of proving the existence of *new* velocity cross-correlation functions, it does not matter if we use $v_\alpha(t)v_\beta(0)$ or $\tilde{v}_\alpha(t)\tilde{v}_\beta(0)$. In shear and elongational flow, the laboratory frame velocity is origin dependent. Also in transient flows the laboratory frame velocity is discontinuous at $t = 0$, the time at which the change in flow rate is made. Therefore the *magnitude* of the *laboratory* frame correlation functions is not well-defined. In contrast, the *peculiar* velocity frame correlation functions are well-defined. This is the reason why we report correlation functions here based on the peculiar velocities.

Examples of asymmetric c.c.f.'s derived from these equations of motion are shown in figs. (2) and (3). In these figures the symmetric component (the "deformation") dominates over the anti-symmetric component (" vorticity"). Consistent results were obtained in the liquid and gaseous states using both SLLOD and PUT algorithms with samples of 108 and 500 atoms. Principle (3) also allows similar off-diagonal asymmetric c.c.f.'s of other atomic dynamic variables, such as atomic position and pressure tensor [51,52] $P_{\alpha\beta}$, and in general any c.c.f. which is overall positive to parity inversion in the point group $R_h(3)$. (In the point group R(3) of an ensemble of chiral molecules, shearing may produce many more c.c.f.'s which are negative to parity inversion in $R_h(3)$. This has yet to be explored, in common with all molecular liquids.) Asymmetric correlation functions of the pressure tensor appear under shear flow of the generic type $\langle P_{\alpha\beta}(t)P_{XY}(0)\rangle$ or $\langle P_{\alpha X}(t)P_{\beta Y}(0)\rangle$ [51,52], providing the first explanation of the Weissenberg effect on the fundamental level. An example of the latter type is given in fig. 4.

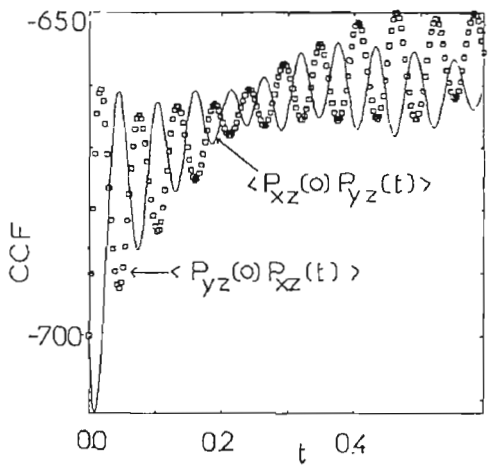

Fig. 4. The time cross-correlation function $(V/k_BT)\langle P_{XZ}(0)P_{YZ}(t)\rangle$, solid line and $(V/k_BT)\langle P_{YZ}(0)P_{XZ}(t)\rangle$, □, using the SLLOD algorithm at the 3D LJ $N = 500$ state, $\rho = 0.8442$, $T = 0.722$ and $\dot{\gamma} = 20$. The simulations are at steady-state shear. The correlation functions are steady state.

The $\langle P_{XZ}(0)P_{YZ}(t)\rangle$ and $\langle P_{XZ}(t)P_{YZ}(0)\rangle$ for the PUT 3D LJ $\rho = 0.8442$, $T = 0.722$, $\dot{\gamma} = 20.0$ and $N = 500$ state are shown in fig. 4. They both start from a finite negative value and then decay in an oscillatory manner with frequency $\nu \approx \dot{\gamma}$. This oscillatory structure we attribute to the formation of a "string" phase in which the molecules travel along the streamlines in lines packed together in a triangular lattice when viewed in cross-section in fig. 1. (The PUT algorithm induces a string phase in 3D for these finite periodic systems in contrast to the case for 2D fluids [19].) Adjacent molecules in neighbouring strings are separated by a distance $\sim \sigma$. The relative velocity between these molecules in the streaming direction is $\sim \sigma\dot{\gamma}$. Hence the frequency with which neighbouring strings have atoms adjacent in the XY plane or "frequency of registry" of molecules is $\sim \dot{\gamma}$. Irrespective of the wider debate concerning the existence of the string phase in monatomic fluids, this figure is noteworthy because the time-reversed function, $\langle P_{YZ}(0)P_{XZ}(t)\rangle$, is significantly different, being neither symmetric nor anti-symmetric to $\langle P_{XZ}(0)P_{YZ}(t)\rangle$. This can be traced to the contribution and dominance of the vorticity component of the flow, which unlike the pure strain component of the strain rate tensor, causes negative to time reversal. (Calculations with $N = 108$ produced the same time-reversal asymmetry, revealing that this effect is independent of N.) The Weissenberg effect is the pressure generated perpendicular to the plane of shear, and this is explained in the computer simulation on the basis of cross correlation between the XY and ZZ elements of the pressure tensor, a direct consequence of principle (3) and the symmetry of the field of force generated by the external shearing stress.

4. Transient flows and elongation

The external force field generating elongational (or laminar) flow is of $D_g^{(0)}$ symmetry, that of the scalar product of v and r^{-1}. By principle (3) elongational flow generates ensemble averages of the same symmetry, the diagonal elements of $\langle v(t)v(0)\rangle$, symmetric to time reversal. The observable effect of elongational stress in general is therefore to change the time dependence of each of these diagonal elements. This again is precisely what is observed by computer simulation [19], where, for the first time, molecular dynamics was used to investigate complicated flows generated by a mixture of elongation and shear. Under elongational stress, the indicator c.c.f. does not develop off-diagonal elements; under shear stress the indicator c.c.f. is purely off-diagonal and asymmetric.

The D symmetry in this case is the complete $D_g^{(0)} + D_g^{(1)} + D_g^{(2)}$, allowing the appearance of both symmetric diagonal elements and asymmetric off-diagonal elements of the indicator c.c.f., for example $\langle v(t)v(0)\rangle$. The detailed time evolution of diagonal and off-diagonal elements is mutually interdependent [19] and one type of flow influences the other.

The elongational flow lines are specified by, $\partial v_X/\partial X$, $\partial v_Y/\partial Y$ and $\partial v_Z/\partial Z$. Within the usual restriction of the simulation cells containing $N \approx 10^2$–10^3 molecules, a *steady-state* elongational flow cannot be achieved for a sufficiently long time to obtain reasonable statistical averages. In previous simulations of elongational flow, this was overcome by implementing a series of transient elongational flows (lasting for 3–4 ps for Ar) starting from different points in equilibrium phase space [9,10]. A series of short-lived steady states was achieved for the purpose of averaging. At the small strain rates considered here a steady state can be achieved before the end of the transient, making this approach suitable for investigating non-Newtonian steady states. This approach is applied here.

The equations for elongational flow are similar to those for shear flow,

$$\dot{R}_X = v_X = \tilde{v}_X + \dot{\gamma}_X R_X, \tag{22}$$

$$\dot{R}_Y = v_Y = \tilde{v}_Y + \dot{\gamma}_Y R_Y, \tag{23}$$

$$\dot{R}_Z = v_Z = \tilde{v}_Z + \dot{\gamma}_Z R_Z, \tag{24}$$

$$\frac{\mathrm{d}\tilde{v}_X}{\mathrm{d}t} = \frac{F_X}{m} - \dot{\gamma}_X \tilde{v}_X, \tag{25}$$

$$\frac{\mathrm{d}\tilde{v}_Y}{\mathrm{d}t} = \frac{F_Y}{m} - \dot{\gamma}_Y \tilde{v}_Y, \tag{26}$$

and

$$\frac{\mathrm{d}\tilde{v}_Z}{\mathrm{d}t} = \frac{F_Z}{m} - \dot{\gamma}_Z \tilde{v}_Z. \tag{27}$$

As for shear flow, thermostatting was performed using velocity rescaling. For convenience, we define $\dot{\gamma}_X = \dot{\gamma}_T \delta_X$, $\dot{\gamma}_Y = \dot{\gamma}_T \delta_Y$ and $\dot{\gamma}_Z = \dot{\gamma}_T \delta_Z$. Elongational flow has $\delta_X = 1$, $\delta_Y = -\frac{1}{2}$ and $\delta_Z = -\frac{1}{2}$ or any permutation of this sequence. We consider here two elongational strain geometries:
(i) $\delta_X = 1$, $\delta_Y = -\frac{1}{2}$ and $\delta_Z = -\frac{1}{2}$;
(ii) $\delta_X = -\frac{1}{2}$, $\delta_Y = 1$ and $\delta_Z = -\frac{1}{2}$.
We calculated the tensile viscosity, η_T, from,

$$\eta_T = \sum_\alpha \delta_\alpha \frac{P_{\alpha\alpha}}{\dot{\gamma}_T}, \tag{28}$$

where,

$$P_{\alpha\alpha} = \frac{1}{V}\left(\sum_{i=1}^{N} m_i \tilde{v}_{\alpha i} \tilde{v}_{\alpha i} - \sum_{i=1}^{N-1} \sum_{j>i}^{N} \left(\frac{r_{\alpha ij} r_{\alpha ij}}{r_{ij}} \right) \frac{\mathrm{d}\phi(r_{ij})}{\mathrm{d}r} \right). \tag{29}$$

As the fluid MD cell is periodically repeated in all three dimensions, the elongational flow should only be susceptible to similar finite N artefacts as for shear flow. There is a constraint that must be satisfied in elongational flow, which is absent in the pure shear flow simulations. There is upper limit on $\dot{\gamma}_T$, determined so that none of the cell dimensions, sidelength L, should be less than twice the pair potential truncation distance (i.e. 5 σ) at any time during the elongation transient. (The maximum distortion occurs at the end of the transient, as $L(t)/L(0) = \exp(\gamma_\alpha t)$.) Despite there being this upper bound on $\dot{\gamma}_T$, the range of allowable $\dot{\gamma}_T$ was sufficient to capture Newtonian and non-Newtonian phenomena broadly comparable to those of shear flow up to $\dot{\gamma} \approx 0.5$. The elongational viscosities are obtained by applying eq. (28) in the plateau region of the response, should one be manifest. At high $\dot{\gamma}_T$ the material structurally degrades before a plateau in either shear or elongational stress occurs. The value of this critical $\dot{\gamma}_T$ depends on ρ, T and $\dot{\gamma}$ if shear flow is also involved.

We employed typically 2400 unique starting points in phase space for elongational flow. We considered a selection of $\dot{\gamma}_T = \delta_X = 1$, $\delta_Y = -\frac{1}{2}$ and $\delta_Z = -\frac{1}{2}$. The expansion of the MD cell in the X direction leads to a decrease in P_{XX}. The contraction in the dimensions of the MD cell in the Y and Z directions creates an increase in P_{YY}. (The equilibrium pressure at this $N = 256$ state point is 0.100 ± 0.004. The equilibrium total internal energy per particle is -5.020 ± 0.001.) Figure 5 shows the time development of the *change* in $P_{\alpha\alpha}$ as a result of the elongational strain, $\dot{\gamma}_T = 0.049$. Figure 6 presents $P_{XX} - \frac{1}{2}P_{YY} - \frac{1}{2}P_{ZZ}$ for three values of $\dot{\gamma}_T = 0.049$, 0.098 and 0.197. They yield $\frac{1}{3}\eta_T$ of 3.37, 2.88 and 2.70 ± 0.03, respectively. We use $\frac{1}{3}\eta_T$ as a natural measure of the elongational viscosity, because in the $\dot{\gamma}_T \to 0$ limit then the Navier–Stokes equation gives $\eta = \frac{1}{3}\eta_T$ [11]. This is known as Trouton's rule in the rheological community. At finite strain rates there is no rigorous link between η and η_T, because the two types of strain cause structural changes of different symmetries. (The Newtonian viscosity at this state point is 3.6 ± 0.1 [12].)

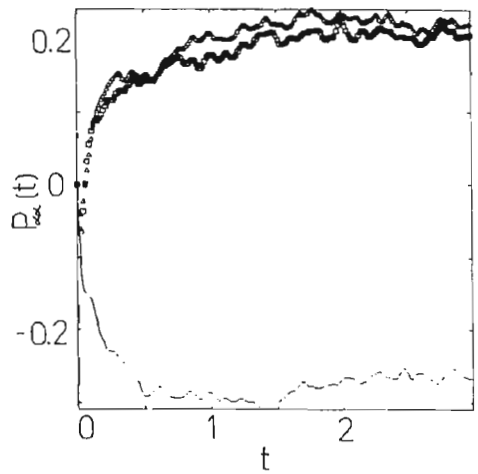

Fig. 5. Elongational flow with $\delta_X = 1$, $\delta_Y = -\frac{1}{2}$ and $\delta_Z = -\frac{1}{2}$. $\partial v_x/\partial y = 0$. The normal pressure responses, $P_{\alpha\alpha}(t)$, of $\rho = 0.8442$, $T = 0.722$, $\dot{\gamma}_T = 0.049$ and $N = 256$ liquids subjected to elongational strain rates applied at time $t = 0$: P_{XX}, solid line, P_{YY}, □, and P_{ZZ}, △. The response functions are transients, with the flow imposed at $t = 0$.

5. Simultaneous elongational and shear flow

We now consider the effects of *simultaneously applied* shear and elongational strain rates. These combined flows produce many non-additive or 11cross effects" in the ensemble averages, such as

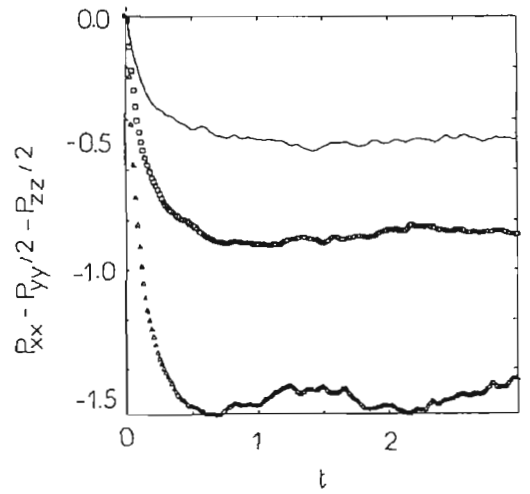

Fig. 6. Elongational flow with $\delta_X = 1$, $\delta_Y = -\frac{1}{2}$ and $\delta_Z = -\frac{1}{2}$. $\partial v_X/\partial y = 0$. The normal pressure responses, $P_{XX}(t) - \frac{1}{2}P_{YY}(t) - \frac{1}{2}P_{ZZ}(t)$, of $\rho = 0.8442$, $T = 0.722$, and $N = 256$ liquids subjected to elongational strain rates applied at time $t = 0$: $\dot{\gamma}_T = 0.049$, solid line, $\dot{\gamma}_T = 0.098$, □, and $\dot{\gamma}_T = 0.197$, △. The response functions are transients, with the flow imposed at $t = 0$.

viscosities and normal pressure effects, manifest also in the cross-correlation functions.

We consider extension in the streaming direction of the shear flow. The strain distortions are defined by $\dot{\gamma}(= \partial v_X/\partial Y)$ and $\delta_X = 1$, $\delta_Y = -\frac{1}{2}$ and $\delta_Z = -\frac{1}{2}$. In fig. 7a the $P_{XY}(t)$ for ($\dot{\gamma} = 0.25$, $\dot{\gamma}_T = 0.0689$) is given. In fig. 7b we show the associated $P_{XX} - \frac{1}{2}P_{YY} - \frac{1}{2}P_{ZZ}$. In these figures $t = 0$ coincides with the commencement of application of the two types of strain rates. The shear stress shows a distinct sign of material failure whereas the elongational stress plateaus out, a complex many-body non-Newtonian phenomenon. P_{XY} at the end of the segment yields $\eta = 2.0 \pm 0.05$, which is significantly lower than the shear viscosity at *this* shear rate in the absence of elongational flow ($= 2.75 \pm 0.04$ [12]). We ascribe this *enhanced* shear thinning to the action of the elongational flow in "dynamically ordering" the fluid along the stream lines of the shear flow (X direction). The elongational flow facilitates the mechanism that causes shear thinning in simple fluids. Under these combined flow circumstances it is not meaningful to characterise this flow in terms of a "viscosity" as there is no plateau in the shear stress. The response is purely viscoelastic.

Computations have also been carried out with an orthogonal or perpendicular relative alignment of the two flow fields, specified by: $\dot{\gamma}(= \partial v_X/\partial Y)$ and $\delta_X = -\frac{1}{2}$, $\delta_Y = 1$ and $\delta_Z = -\frac{1}{2}$. This flow has

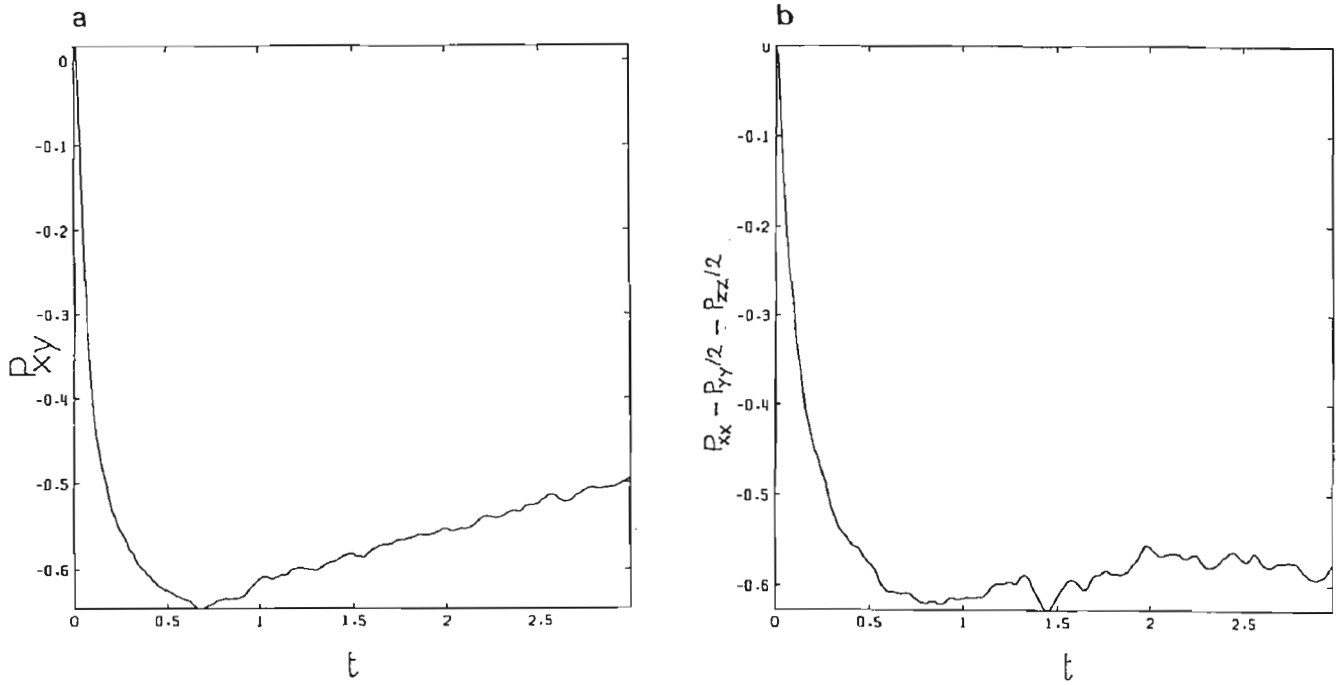

Fig. 7. Combined shear and elongation, where $\dot{\gamma} = 0.25$, $\dot{\gamma}_T = 0.0689$, solid line, (a) $P_{XY}(t)$, (b) $P_{XX}(t) - \frac{1}{2}P_{YY}(t) - \frac{1}{2}P_{ZZ}(t)$ with $\delta_X = 1$, $\delta_Y = -\frac{1}{2}$ and $\delta_Z = -\frac{1}{2}$ for $\rho = 0.8442$ and $T = 0.722$, $N = 256$ liquids subjected to shear strain rates applied at time $t = 0$. The response functions are transients, with the flow imposed at $t = 0$.

the extension of the fluid taking place perpendicular to the streaming (x) direction. This gives rise to the class of "perpendicular" shear and elongational flow combinations. We have considered these two classes of combined flow in order to clarify the general trends. In any practical arrangement, (e.g. flow into a contraction), the flow will be a linear combination of these two classes at different points in the flow field.

This perpendicular flow combination has a quite different effect on the shear viscosity. There is still $\dot{\gamma}$-induced shear thinning in η, when accompanied by a finite $\dot{\gamma}_T$. However, the elongational flow acts to diminish the extent of shear thinning when compared with the unelongated sample. For example, at $\dot{\gamma} = 0.25$ and $\dot{\gamma}_T = 0.049$, $\eta = 2.92$, whereas at the same shear rate but $\dot{\gamma}_T = 0$ we have $\eta = 2.76$ [12]. (Note $\eta = 3.5$ for $\dot{\gamma} \to 0$.) The effect of this class of elongational flow is to compress the particles in the streaming direction. This we suggest, overrides expansion in the y direction, leading to less shear thinning at finite $\dot{\gamma}$ in the presence of "orthogonal" $\dot{\gamma}_T$. We conclude that flow in the non-Newtonian regime is facilitated when the streaming velocities of *both* the shear and elongational strain rates are parallel.

In fig. 8a we present the $P_{\alpha\alpha}$ for two of these flow combinations. In fig. 8a the two flow fields have a comparable effect, but in 8b the shear field dominates (evident in P_{XX} going positive for $t >$ 1.0). The shear flow promotes all diagonal pressure tensor components to become positive. The outcome in any simulation depends on the relative magnitudes of $\dot{\gamma}$ and $\dot{\gamma}_T$ and the competition between the somewhat incompatible preferences of the two flows.

An interesting consequence of principle (3) is that combined elongational and shear stress has the necessary symmetry to generate heat flux and thermal conductivity. This expectation has been confirmed by Molecular dynamics simulation [19] thus proving the existence of a new effect, unknown to rheology. In this context [19], thermal conductivity is defined as the Green–Kubo in-

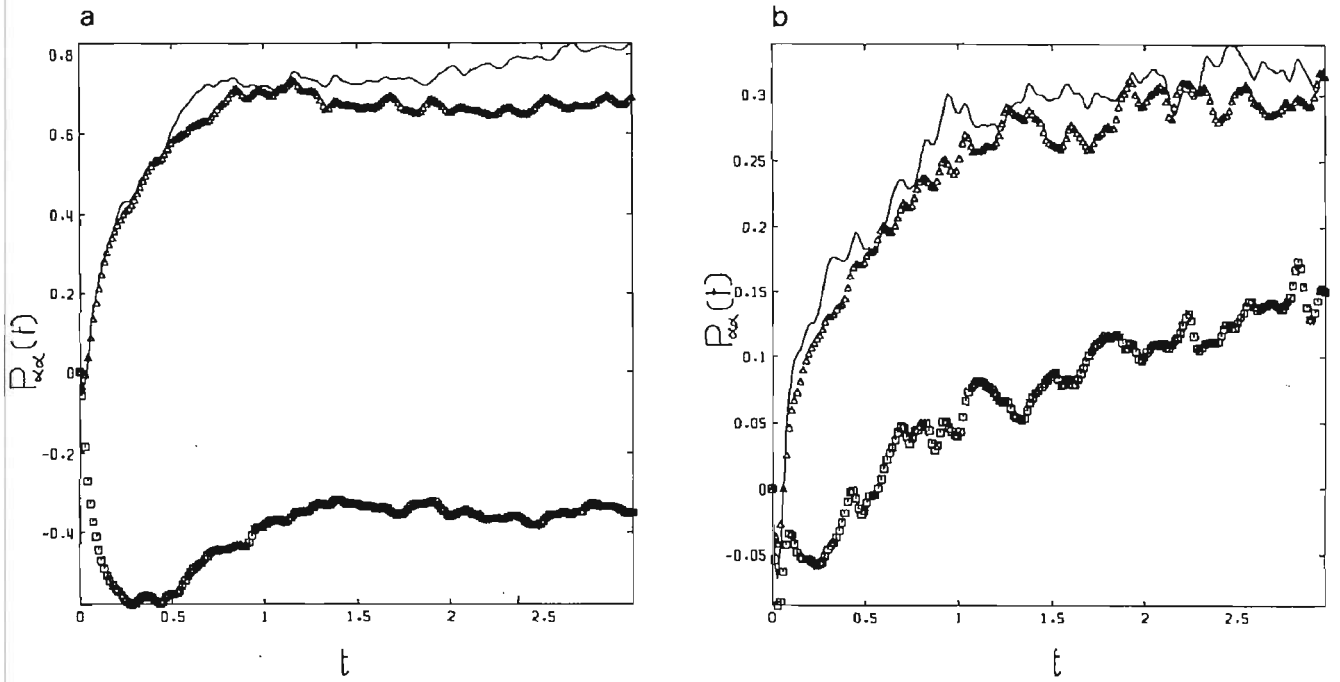

Fig. 8. A combination of shear flow, $\dot{\gamma} = \partial v_X/\partial Y$, and elongational flow with $\delta_X = -\frac{1}{2}$, $\delta_Y = 1$ and $\delta_Z = -\frac{1}{2}$. The $P_{\alpha\alpha}$ time responses of $\rho = 0.8442$, $T = 0.722$, and $N = 500$ liquids. Key: P_{XX}, solid line; P_{YY}, □, and P_{ZZ}, △. (a) $\dot{\gamma} = 0.25$ and $\dot{\gamma}_T = 0.1477$, (b) $\dot{\gamma} = 0.25$ and $\dot{\gamma}_T = 0.0246$. The response functions are transients, with the flow imposed at $t = 0$.

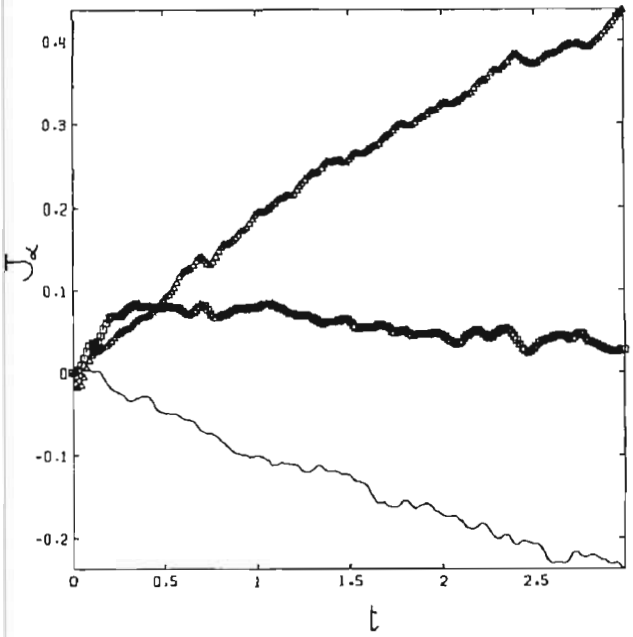

Fig. 9. A combination of shear flow, $\dot{\gamma} = \partial v_X/\partial Y$, and elongational flow with $\delta_X = 1$, $\delta_Y = -\frac{1}{2}$ and $\delta_Z = -\frac{1}{2}$. The heat current J_α time responses of $\rho = 0.8442$, $T = 0.722$, and $N = 256$ liquids with $\dot{\gamma} = 0.25$ and $\dot{\gamma}_T = 0.049$: J_X, solid line, J_Y, □, and J_Z, △. The response functions are transients, with the flow imposed at $t = 0$.

tegral over the correlation function of the Irving–Kirkwood heat flux tensor. The complete symmetry of the correlation function is

$$\left(D_u^{(1)} D_u^{(1)}\right)^3 = \left(D_g^{(0)} + D_g^{(1)} + D_g^{(2)}\right)^3, \qquad (30)$$

i.e. the cube of the D symmetry of the external force field equivalent to combined elongational and shear stress. Thermal conductivity in frame (X, Y, Z) is generated by this complete symmetry only, and does not appear computationally [58] when either elongational or shear stress is absent. The appearance of thermal conductivity from the computer simulation is illustrated in fig. 9.

In transient flows the non-equilibrium cross-correlation functions, $\langle \tilde{v}_X(s)\tilde{v}_Y(0)\rangle$ and $\langle \tilde{v}_Y(s)\tilde{v}_X(0)\rangle$ also appear in response to shear. Here the time argument 0 is taken from an equilibrium ensemble and s from the transient flow state. The observed transients are weighted sums of the vorticity and deformational transients. Rise transients and fall transient c.c.f.'s of velocity can be defined in the non-equilibrium condition. The former occur immediately after a field is applied at the equilibrium point $t = 0$. The non-equilibrium c.c.f. is built up with one variable in the equilibrium condition and the other in the rise transient condition at $t = s$, for example $\langle \tilde{v}_X(0)\tilde{v}_Y(s)\rangle$. Fall transient c.c.f.'s are defined with $\tilde{v}_Y$ having reached the field-on steady state. After reaching the steady state the field is switched off at $t = 0$ and the non-equilibrium c.c.f. constructed by correlating $\tilde{v}_Y$ at this instant with $\tilde{v}_X$ in the fall transient condition at $t = s$. The c.c.f. is therefore $\langle \tilde{v}_Y(0)\tilde{v}_X(s)\rangle$. We see that one c.c.f. is generated from the other by a time or index reversal. The velocity rise and fall transients are *asymmetric* and become approximately symmetric only when the external field goes to zero. The rise and fall transient velocity c.c.f.'s cannot have the same time dependence. The rise transients are obtained with $t = 0$ of the transient c.c.f. at equilibrium (field off) and $t = s$ in the transient condition after application of shear. The fall transients are obtained with $t = 0$ of the transient c.c.f. at steady state in the presence of shear, and $t = s$ in the transient state after *removing* the shear. The transients are sums of the vorticity and deformational parts and the overall asymmetry means that the time dependence of the rise and fall transients cannot be the same. The velocity transient c.c.f.'s are molecular probes of the non-Newtonian nature of the sheared ensemble. With this observation we have fused together rheology, dielectric and the dynamical Kerr effect.

In fig. 10 we show the *difference* in the transient c.c.f.'s, $\langle \tilde{v}_X(0)\tilde{v}_Y(t)\rangle$, in rise and fall conditions. That is, for the rise situation the c.c.f. is $\langle \tilde{v}_X(0)\tilde{v}_Y(t)\rangle_{\dot{\gamma}} - \langle \tilde{v}_X(0)\tilde{v}_Y(t)\rangle_{\dot{\gamma}=0}$, where at time $t = 0$ the two ensembles depart due to the different strain rate histories. The "background" steady state is unsheared fluid. For the fall situation the c.c.f. is $\langle \tilde{v}_X(0)\tilde{v}_Y(t)\rangle_{\dot{\gamma}=0} - \langle \tilde{v}_X(0)\tilde{v}_Y(t)\rangle_{\dot{\gamma}}$. In this case we have the reverse situation of a steady-state sheared fluid and an instantaneously "applied" unsheared state. The two difference c.c.f.'s in fig. 10a are clearly quite different. The corresponding "difference" mean square displacements in the x ("streaming") direction are shown in fig. 10b. (The position increments due to the peculiar momenta are only used.) This figure shows that the presence of shear causes enhanced self-diffu-

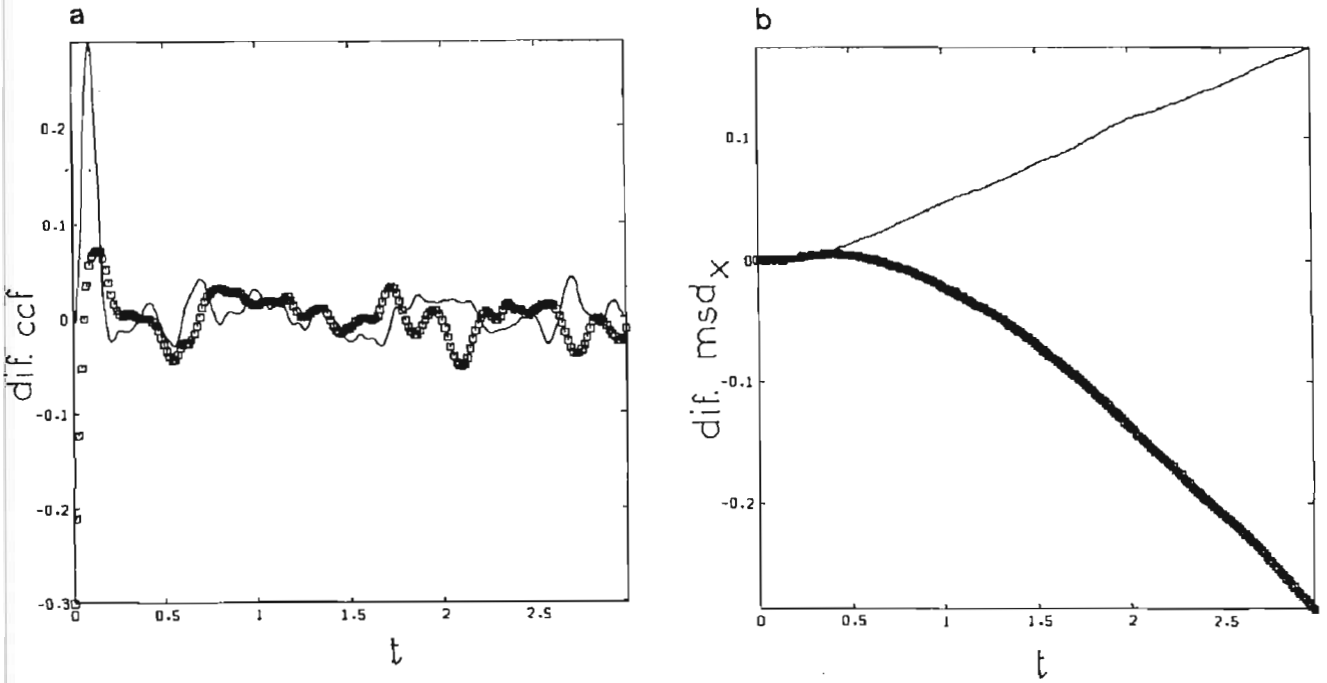

Fig. 10. (a) The difference c.c.f.'s in rise and fall transients ($\dot{\gamma} = 3$). The solid line is for the rise and the squares are for the fall. (b) The corresponding difference mean square displacement (m.s.d.) in the x direction.

sion, whether in a steady or transient state compared to the unsheared state. The corresponding y and z m.s.d. curves are all positively increasing, indicating that any sudden change of shear rate (application or cessation) to a fluid causes at least a temporary enhancement of self-diffusion in the y and z directions.

Rise transients and fall transients of shear induced velocity provide information analogous to that in orientational transients induced by an electric field [58]. The latter depend on field strength when the response is non-linear. The rise transients show field induced oscillations, recently confirmed by computer simulation [58], and the fall transients are accelerated with respect to the equivalent equilibrium correlation function. The latter is an exclusive indicator of non-linear response, and is also expected to occur in the contexts of shear and elongational flow. Oscillations in the rise transient are indicative [59] of non-Markovian, non-linear statistical mechanics.

6. Shear induced depolarised light scattering

The indication by computer simulation of entirely new types of asymmetric correlation function implies the need for experimental observation. One of the most direct routes is by light scattering, because the Fourier transform of the second moment of the light scattering spectrum is a current correlation function of the type,

$$C_3(t) = \langle \tilde{v}(t)\tilde{v}(0) \exp(i\boldsymbol{q}\cdot(\boldsymbol{r}(t) - \boldsymbol{r}(0))\rangle, \quad (31)$$

where

$$\boldsymbol{r}(t) - \boldsymbol{r}(0) = \int_0^t \boldsymbol{v}(t)\, dt, \quad (32)$$

and $\boldsymbol{q}$ is the scattering vector [60], $\boldsymbol{q} = \boldsymbol{k} - \boldsymbol{k}_0$. The symmetry representation of the current correlation function in frame (X, Y, Z) is the same as that of the indicator c.c.f. $\langle \tilde{v}(t)\tilde{v}(0)\rangle$, because the exponential multiplier is a scalar. Applying principle (3) we see that a shearing field must induce asymmetric off-diagonal components of $C_3(t)$, and that an elongational field produces symmetric diagonal elements.

Principle (3) indicates that shear stress produces an asymmetric *depolarised* light scattering

spectrum, related by Fourier's integral theorem to the equivalent correlation function of the type,

$$C_4(t) = \langle \tilde{v}_X(t)\tilde{v}_Y(0)\exp(i\boldsymbol{q}\cdot(\boldsymbol{r}(t)-\boldsymbol{r}(0))\rangle, \tag{33}$$

$$C_4(t) \neq \langle \tilde{v}_Y(t)\tilde{v}_X(0)\exp(i\boldsymbol{q}\cdot(\boldsymbol{r}(t)-\boldsymbol{r}(0))\rangle, \tag{34}$$

and elongational stress produces a *polarised* light scattering spectrum involving the symmetric diagonal components equivalent to $C_4(t)$. A combination of both shear and elongational stress affects both the polarised and depolarised parts of the second-momentum spectrum. The specific effect of the elongational component on the shear component can be observed in the depolarised component, which vanishes in the absence of shear.

The correlation function $C_4(t)$ has been isolated quantitatively by a recent computer simulation and shows the asymmetry predicted by principle (3). We note that the light scattering spectrum is the second moment of the observed light scattering intensity, i.e. the latter multiplied by the square of the angular frequency. The depolarised second-moment spectrum is related specifically to the appropriate off-diagonal elements of the shear-induced indicator function $\langle \tilde{v}(t)\tilde{v}(0)\rangle$ through the current correlation function, and disappears at thermodynamic equilibrium. This new type of spectrum is obtained straightforwardly from a direct application of principle (3). The collective correlation functions are derived from eqs. (33) and (34) using,

$$S_{qX} = \sum_{i=1}^{N} \tilde{v}_{Xi}\sin(q_X r_{Xi} + q_Y r_{Yi}), \tag{35}$$

$$S_{qY} = \sum_{i=1}^{N} \tilde{v}_{Yi}\sin(q_X r_{Xi} + q_Y r_{Yi}). \tag{36}$$

Here the velocities are excess or "peculiar" velocities, being the velocity deviation from the local spacial average. From eqs. (35) and (36) we can construct a number of component collective correlation functions,

$$S_{qXY}(t) = \langle s_{qX}(0)s_{qY}(t)\rangle, \tag{37}$$

$$S_{qYX}(t) = \langle s_{qY}(0)s_{qX}(t)\rangle. \tag{38}$$

These functions are used in calculating the real and imaginary parts of the frequency transforms. In fig. 11 we give a typical example of S_{qXY} and S_{qYX}, for $\dot{\gamma} = 0, 1, 2$ and $\boldsymbol{q}^* = (q_x^*, q_y^*, q_z^*) =$

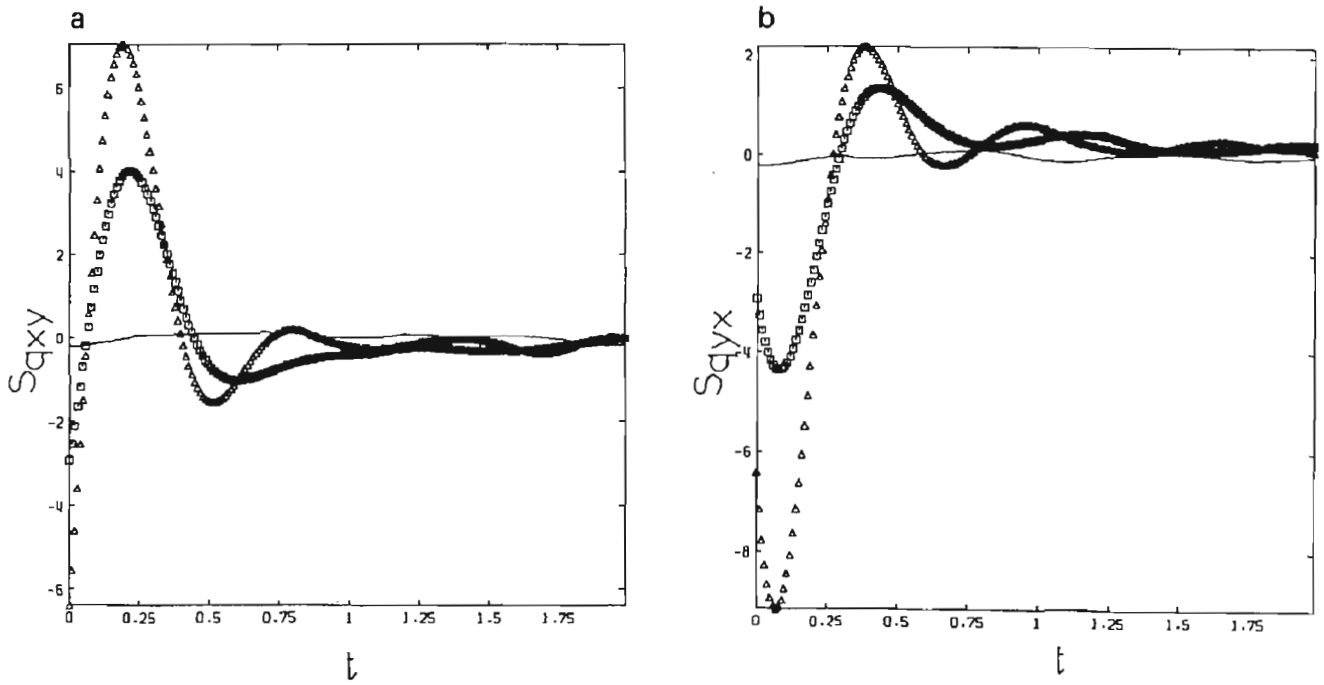

Fig. 11. (a) $S_{qXY}(t)$, (b) $S_{qYX}(t)$, for $\dot{\gamma} = 0, 1, 2$ and $\boldsymbol{q}^* = (q_x^*, q_y^*, q_z^*) = (0, 1.25, 0)$; $\dot{\gamma} = 0$, solid line; $\dot{\gamma} = 1$, □; $\dot{\gamma} = 2$, △.

(0, 1.25, 0). It shows that shear flow creates a non-zero time correlation function, which increases in magnitude with shear rate. (At $\dot{\gamma} = 1$ and 2, $\eta = 2.06$ and 1.66, respectively.)

7. Flow in molecular liquids

Principle (3) applied to shear stress in molecular liquids implies the possible existence of many more asymmetric correlation functions of the generic type $\langle A(t)A(0)\rangle$ or $\langle A(t)B(0)\rangle$, provided that A and B have the same parity reversal symmetry in $R_h(3)$. In the point group R(3) of chiral molecules this condition becomes superfluous, providing the possibility of shear-induced cross-correlation functions such as $\langle v(t)\omega(0)\rangle$, which are negative to parity reversal in $R_h(3)$. In general these are again asymmetric, being a weighted combination of $D^{(1)}$ and $D^{(2)}$ symmetry.

In the presence of shear, it is possible by principle (3) to generate the asymmetric c.c.f. $\langle \mu_X(t)\mu_Y(0)\rangle \neq \langle \mu_Y(t)\mu_X(0)\rangle$ where μ is the molecular permanent dipole moment. Fourier transformation relates this to a dielectric spectrum [59,60], consisting of a frequency dependent dielectric loss and permittivity. This spectrum contains information on deformation and vorticity and is asymmetric in the indices of the shear plane. The range of frequencies over which the shear-induced dielectric loss is non-zero can be made to coincide with the shearing frequencies attainable experimentally, currently up to the MHz range. The maximum experimental effect is likely to occur when the dielectric-loss peak frequency coincides with the frequency of shear, and this can be adjusted using appropriate samples, temperature and pressure, from Hz to MHz, providing plenty of scope for experimental investigation.

Programs for the investigation of shear-induced c.c.f.'s in molecular liquids are currently under development, and should result in a wide variety of new insights, suggesting the existence of new types of spectral investigation of non-Newtonian features such as shear-induced thinning, thickening and vorticity. Ultimately, these methods will probably be of direct analytical value in industrial laboratories for the development of new materials, and for the investigation of fundamental rheology in very non-Newtonian materials such as liquid crystals.

To date, agreement has been obtained on the existence of asymmetric correlation functions using different programs (SLLOD, PUT, and BD) and different numbers of atoms in the ensemble (up to 500). Using symmetry principles as a guide, new spectral techniques are suggested by the simulated asymmetric c.c.f.'s. These results are inaccessible to customary hydrodynamics even in the simplest of liquids, consisting of atomic ensembles, but show great promise if extended to structured fluids, where the problems of the customary approach are greatly compounded and confused by ill-defined constitutive equations and by contemporary controversy such as that over frame indifference. In contrast, the symmetry principles of this paper are simple enough to go beyond controversy of this kind, yet powerful enough to result in insights overlooked completely in classical hydrodynamics. An example of these is the demonstration by MD simulation of the appearance of thermal conductivity specific to combined shear and elongational flow. This thermal conductivity can be measured experimentally and used as an indicator of the way in which shear and elongational stresses are mutually influential. This type of finding is clearly of interest in industrial contexts, for example in tracing the weak points (and weak contours) of a structure under complicated stresses by the changes in thermal conductivity, picked up perhaps by sensitive heat detectors such as arrays of Golay detectors. This structure could be anything from a fibre composite to a turbine blade to an aircraft wing to a suspension bridge.

Acknowledgements

D.M.H. gratefully thanks The Royal Society for the award of a Royal Society 1983 University Research Fellowship. MWE is grateful to the Academic Board of RHBNC for the award of an Honorary Research Fellowship. Many colleagues and friends are thanked for suggestions and useful discussions. We thank S.E.R.C. for the award of computer time at the University of London Com-

puter Centre, and the RHBNC Computer Center for use of their VAX 11/780 computer facilities.

References

[1] J. Harris, Rheology of Non-Newtonian Flow (Longman, London, 1977).
[2] B.C. Eu, J. Chem. Phys. 82 (1985) 3773.
[3] A.S. Lodge, R.B. Bird, C.F. Curtiss and M.W. Johnsson, J. Chem. Phys. 85 (1986) 2341.
[4] R. Zwanzig, Proc. Nat. Acad. Sci. 78 (1981) 3296.
[5] B.C. Eu, J. Chem. Phys. 85 (1986) 2342.
[6] D.J. Evans and G.P. Morriss, Comput. Phys. Rep. 1 (1984) 297.
[7] D.J. Evans and G.P. Morriss, Chem. Phys. 87 (1984) 451.
[8] D.J. Evans and G.P. Morriss, Phys. Rev. A 30 (1984) 1528.
[9] B.L. Holian and D.J. Evans, J. Chem. Phys. 83 (1985) 629.
[10] D.J. Evans and G.P. Morriss, Phys. Rev. Lett. 56 (1986) 2172.
[11] D.M. Heyes, Comput. Phys. Rep. 8 (1988) 71.
[12] D.M. Heyes, J. Chem. Soc. Faraday Trans. II 82 (1986) 1365.
[13] D.M. Heyes, Chem. Phys. 98 (1985) 15.
[14] D.M. Heyes, Physica A 146 (1987) 341.
[15] D.M. Heyes and L.V. Woodcock, Mol. Phys. 59 (1986) 1369.
[16] D.M. Heyes, J. Chem. Soc. Faraday Trans. II 83 (1987) 1985.
[17] D.L. Ermak and J.A. McCammon, J. Chem. Phys. 69 (1978) 593.
[18] D.M. Heyes, Comput. Phys. Rep., 8 (1988) 71.
[19] M.W. Evans and D.M. Heyes, Mol. Phys. 69 (1990) 241.
[20] D.M. Heyes and R. Szczepanski, J. Chem. Soc. Faraday Trans. II 83 (1987) 319.
[21] J. Chamberlain, Principles of Interferometric Spectroscopy (Wiley, Chichester, 1978).
[22] G. Chantry, Submillimetre Spectroscopy (Academic, New York, 1971).
[23] M.W. Evans, G.J. Evans, W.T. Coffey and P. Grigolini, Molecular Dynamics (Wiley/Interscience, New York, 1982).
[24] M.W. Evans, ed., Dynamical Processes in Condensed Matter, Advances in Chemical Physics, Series vol. 63, ser. eds. I. Prigogine and S.A. Rice (Wiley/Interscience, New York, 1985).
[25] G.P. Morriss and D.J. Evans, Phys. Rev. A 35 (1987) 792.
[26] M.W. Evans, Chem. Phys. Lett. 152 (1988) 33.
[27] M.W. Evans, Chem. Phys. 127 (1988) 413.
[28] M.W. Evans, Chem. Phys. 132 (1989) 1.
[29] M.W. Evans, Phys. Lett. A 134 (1989) 409.
[30] M.W. Evans, Chem. Phys. Lett. (1989).
[31] M.W. Evans, Physica B 154 (1989) 313.
[32] R.L. Flurry Jr., Symmetry Groups, Theory and Chemical Applications (Prentice-Hall, Englewood Cliffs, NJ, 1980).
[33] F.A. Cotton, Chemical Applications of Group Theory (Wiley/Interscience, New York, 1963).
[34] D.S. Urch, Orbitals and Symmetry (Penguin Books, Harmondsworth, 1970).
[35] L.D. Barron, Chem. Soc. Rev. 15 (1986) 189.
[36] F.E. Neumann, Vorlesungen uber die Theorie Elastizitat der Festen Korper und dem Lichtathers (Teubner, Leipzig, 1885).
[37] P. Curie, J. Phys. (Paris) 3 (1894) 393.
[38] D.H. Whiffen, Mol. Phys. 63 (1988) 1053.
[39] M.W. Evans and D.M. Heyes, Phys. Scr. 41 (1990) 304.
[40] M.W. Evans and D.M. Heyes, J. Mol. Liq. 44 (1989) 27.
[41] M.W. Evans and D.M. Heyes, J. Mol. Liq. 44 (1989) 39.
[42] M.W. Evans, G.C. Lie and E. Clementi, J. Chem. Phys. 89 (1988) 6399.
[43] M.W. Evans, G.C. Lie and E. Clementi, J. Mol. Liq. 37 (1988) 231.
[44] M.W. Evans, G.C. Lie and E. Clementi, Phys. Rev. A 37 (1988) 2548.
[45] M.W. Evans, G.C. Lie and E. Clementi, J. Chem. Phys. 88 (1988) 5157.
[46] M.W. Evans, G.C. Lie and E. Clementi, Z. Phys. D 7 (1988) 397.
[47] J.K. Moscicki, in: Dynamical Processes in Condensed Matter, M.W. Evans, ed. (Wiley/Interscience, New York, 1985) p. 631.
[48] M.W. Evans, Phys. Lett. A 102 (1984) 248.
[49] M.W. Evans, Phys. Scr. 31 (1985) 419.
[50] M.W. Evans, Physica B & C 131 (1985) 273.
[51] M.W. Evans and D.M. Heyes, Mol. Phys. 65 (1988) 1441.
[52] M.W. Evans and D.M. Heyes, J. Chem. Soc. Faraday Trans. II 86 (1990) 1041.
[53] M.W. Evans and D.M. Heyes, Mol. Sim. 4 (1990) 304.
[54] M.W. Evans and D.M. Heyes, Phys. Scr. 42 (1990) 96.
[55] M.W. Evans and D.M. Heyes, J. Mol. Liq. 40 (1989) 115.
[56] D. MacGowan and D.M. Heyes, Mol. Simulation 1 (1988) 277.
[57] H.J.M. Hanley, G.P. Morriss, T.R. Welberry, and D.J. Evans, Physica A 149 (1988) 406.
[58] M.W. Evans, G.C. Lie and E. Clementi, Phys. Lett. A 130 (1988) 289.
[59] B.J. Berne and R. Pecora, Dynamical Light Scattering with Applications to Chemistry, Physics and Biology (Wiley/Interscience, New York, 1976).
[60] N. Hill, W. Vaughan, A.H. Price, and M. Davies, Dielectric Properties and Molecular Behaviour (Van Nostrand/Rheinholdt, London, 1969).